A combined etching process toward robust superhydrophobic SiC surfaces

2012 Nanotechnology 23 255703

(http://iopscience.iop.org/0957-4484/23/25/255703)

Nanotechnology **23** (2012) 255703 (7pp) doi:10.1088/0957-4484/23/25/255703

A combined etching process toward robust superhydrophobic SiC surfaces

Yan Liu[1], Wei Lin[1], Ziyin Lin[1], Yonghao Xiu[1] and C P Wong[1,2]

[1] School of Materials Science and Engineering, Georgia Institute of Technology, 771 Ferst Drive, Atlanta, GA 30332-0245, USA
[2] Faculty of Engineering, The Chinese University of Hong Kong, Shatin, NT, Hong Kong

E-mail: cp.wong@mse.gatech.edu

Received 19 December 2011, in final form 9 May 2012
Published 31 May 2012
Online at stacks.iop.org/Nano/23/255703

Abstract
Large-scale porous SiC was fabricated by a combination of Pt-assisted etching and reactive ion etching. It was found that the surface roughness of combined etchings increased dramatically in comparison with metal-assisted etching or reactive ion etching only. To reduce the surface energy, the porous SiC surface was functionalized with perfluorooctyl trichlorosilane, resulting in a superhydrophobic SiC surface with a contact angle of 169.2° and a hysteresis of 2.4°. The superhydrophobicity of the SiC surface showed a good long-term stability in an 85 °C/85% humidity chamber. Such superhydrophobicity was also stable in acidic or basic solutions, and the pH values showed little or no effect on the SiC surface status. In addition, enhancement of porosity-induced photoluminescence intensity was found in the superhydrophobic SiC samples. The robust superhydrophobic SiC surfaces may have a great potential for microfluid device, thermal ground plane, and biosensor applications.

S Online supplementary data available from stacks.iop.org/Nano/23/255703/mmedia

(Some figures may appear in colour only in the online journal)

1. Introduction

Silicon carbide (SiC) has unique physical properties such as wide bandgap, high breakdown electric fields, high electron saturation velocity, and high thermal conductivity [1]. It has promising applications for high power semiconductor microelectronics, bright blue LED photodiodes, sensors, etc [2, 3]. The reliability of SiC-based devices is an important issue in practical applications, yet has rarely been addressed in the literature. One of the general and most important issues for semiconductor device reliability is water/moisture uptake/absorption [4]. It has been proposed that introducing hydrophobicity or superhydrophobicity to semiconductor surfaces will improve the device reliability and performance under hostile environments, such as high humidity, chemical contamination and thermal stress [5].

Superhydrophobic surfaces, which display water contact angles larger than 150° with self-cleaning properties [6–8], have been widely used in anti-stiction and anti-contamination films in opto-electronics, biochemical sensors, and micro-electromechanical systems (MEMS). To prepare a superhydrophobic SiC surface, surface chemistry and roughness are the two key factors to manipulate [9–12]. Surface chemistry of SiC can be tailored relatively easily by chemical modifications [13]. In comparison, surface roughness control of SiC has been fairly difficult mainly due to the high chemical stability of Si–C bonds. Although superhydrophobicity has been reported for films/nets composed of surface-modified SiC nanowires on Si wafer [13, 14], where the surface roughness was realized by synthesized nanowires, no success has ever been reported on creating a superhydrophobic surface on a bulk SiC.

To generate desired surface roughness on a bulk SiC, wet chemical etching and dry etching are feasible [1, 15, 16]. Wet chemical etching of SiC can be realized in alkaline solutions at elevated temperatures, or with photoelectrochemical etching at room temperature [1, 17, 18]. The need for high temperature (typically higher than 600 °C) and electrical contacts in the anodization process limits the large-scale production of etched SiC [19]. Alternatively, electroless chemical etching with

metal catalysts, called metal-assisted etching (MAE), has been developed [16, 20]. Platinum (Pt) is a typical catalyst for MAE of SiC [21, 22]. Rittenhouse *et al* [20] used a solution containing HF and $K_2S_2O_8$ as the etchant to generate porous SiC structure. In the Pt-assisted etching process, UV illumination injects holes in the valence band of SiC, and then the holes are involved in the oxidation process.

Being different from the wet chemical etching, dry etching such as reactive ion etching (RIE) [23] has the capability of etching SiC precisely and anisotropically in both large and small dimensions [24]. RIE in fluorinated plasma has been widely applied for electronic device fabrication at room temperature. Both physical and chemical processes occur during the etching. It is reported that SiC RIE in fluorine-based plasmas produce anisotropic etching and submicron patterning with etching rate 100–1000 Å min^{-1}. The etchant gases such as CHF_3, $CBrF_4$, CF_4, SF_6, and NF_3 are commonly used [24].

In the present study, we develop an efficient etching method by combining MAE and RIE, which can be used for large-scale fabrication of a porous SiC surface. The surface roughness and air trapping volume are enhanced significantly through the combined etching. After surface functionalization of the etched SiC with perfluorooctyltrichlorosilane (PFOS), the contact angle increases up to ∼170° with a small contact angle hysteresis of 2.4°. The superhydrophobicity of the SiC surface is highly stable under hostile environment, such as in an 85 °C/85% humidity chamber and corrosive acid/base solutions. Moreover, the luminescent intensity of porous superhydrophobic SiC is enhanced in comparison with the pristine bulk SiC.

2. Experimental details

The Pt-assisted etching was performed using HF and $K_2S_2O_8$ etchant at room temperature. 10 nm Pt was coated on a 6H n-type SiC wafer using the e-beam evaporation method. The wet etchant used was concentrated HF etchant consisting of 6.3 M HF and 0.1 M $K_2S_2O_8$. Ultraviolet irradiation, required to form the porous morphology, was applied using a 150 W Hg arc-lamp. The arc-lamp emission was filtered to expose the wafer to about 32 mW cm^{-2} at full spectrum. The distance between arc-lamp and SiC substrate is 10 cm. After etching, the remaining Pt was removed by sonication in aqua regia for 30 min.

Reactive ion etching (RIE) was conducted on SiC in a plasma thermal reactive ion etcher using fluorinated gas SF_6 and noble gas argon. Etching was operated at 50 mTorr pressure and 150 W power for 30 min. Etching gases were SF_6:Ar = 1:3 (10 sccm SF_6 and 30 sccm Ar). After etching, wafers were cleaned in ethanol.

A 3 mM solution of PFOS in hexane was used for hydrophobic treatment. Specifically, the etched silicon carbide wafers were immersed in the solution for 30 min followed by a heat treatment at 150 °C in air for 1 h to complete the hydrophobic surface modification. Contact angle measurements were performed with a Rame-Hart goniometer that had a CCD camera equipped for image capture. A Leo 1530 scanning electron microscope (SEM) and Veeco Dimension 3100 atomic force microscope (AFM) were used to measure the surface morphology and roughness of porous SiC samples. Thermo K-Alpha x-ray photoelectron spectroscopy (XPS) was carried out for element composition and analysis. The fitting to XPS data was analyzed by XPSPEAK41 software. Photoluminescence was measured in a Shimadzu FP-5301PC spectrofluorometer.

3. Results and discussion

In the MAE process, Pt was deposited on SiC, which assists the chemical etching of SiC in the solution of HF and $K_2S_2O_8$ under UV irradiation. The proposed mechanism is described as follows:
Cathode (Pt):

$$4S_2O_8^{2-} \xrightarrow{hv,\ Pt\ cat} 8SO_4^{-\cdot}$$

$$8SO_4^{-\cdot} + 8e^- \rightarrow 8SO_4^{2-}.$$

Anode (n-tpye SiC):

$$SiC + 4H_2O + 8h^+ \rightarrow SiO_2 + 8H^+ + CO_2$$

$$SiO_2 + 6HF \rightarrow H_2SiF_6 + 2H_2O.$$

Overall:

$$4S_2O_8^{2-} + SiC + 2H_2O + 6HF \rightarrow 8SO_4^{2-} + 8H^+ + CO_2 + H_2SiF_6.$$

The photochemistry of peroxydisulfide was reported by Bardwell *et al* [25]. The portion in the UV light with wavelength shorter than 310 nm generates sulfate radicals from peroxydisulfide. The sulfate radicals are catalytically reduced at the surface of the Pt nanoparticles by obtaining electrons, which generates holes in the valence band of SiC. The holes in the SiC are chemically equivalent to dangling bonds. The dangling bonds are attacked by H_2O, which is a nucleophilic species. The resulting SiO_2 was easily dissolved/etched by HF [26].

3.1. Surface morphology and roughness

The surface morphology has a great influence on the hydrophobicity. SEM and AFM were used as primary tools to investigate the surface morphology and roughness. The pore size and etching depth are studied and discussed in detail to elucidate the characteristics of MAE and RIE in producing surface roughness on SiC.

SEM and AFM analysis in figures 1 and 2 show a porous SiC surface after MAE, and the porosity existed mainly in the near-surface region, confirmed by a small peak to valley depth (table 1). It is found that the surface roughness increased with the etching time (table 2). The mean roughness (R_a) and root mean square roughness (R_q) were both ∼10 nm after 60 min etching. The average feature size of pores was around 150 nm.

Reactive ion etching on SiC was conducted using fluorinated gas SF_6 and Ar. Ar, a typical noble gas, is added to facilitate the ignition of plasma and to enhance the ion-assisted component of the etching. Some reports

Table 1. Roughness of textured SiC using different etching methods measured by AFM.

Etching method	Root mean square roughness (R_q) (nm)	Mean roughness (R_a) (nm)	Maximum peak to valley height (R_{max}) (nm)
MAE only	9.11	7.68	55
RIE only	41.9	33.2	340
MAE + RIE	72.3	59	471

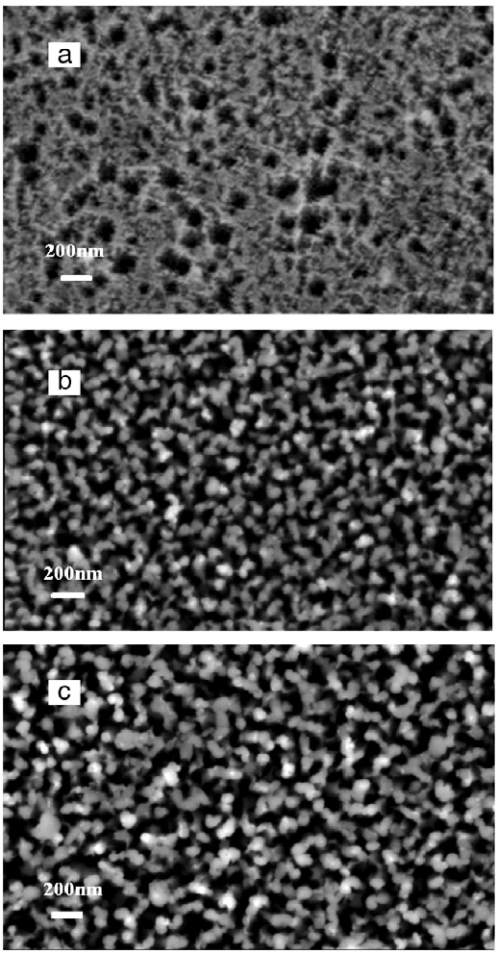

Figure 1. SEM images of SiC using different etching methods (a) MAE, (b) RIE, and (c) combined MAE and RIE.

Table 2. Surface roughness of Pt-assisted etching of SiC for different times.

	MAE-SiC	
Etching time (min)	RMS roughness (R_q) (nm)	Mean roughness (R_a) (nm)
15	1.34	0.93
30	4.24	2.62
60	9.11	7.68

indicate the addition of noble gas enables more efficient power deposition and greater ion/radical production, which also help increase the sheath potential for larger self-biases under the same gas pressure [27, 28]. Compared with MAE, RIE generates a higher density of porous structure and larger etching depth. The R_a was ∼40 nm when etching time was 30 min, and the maximum peak to valley height (R_{max}) increased to 340 nm compared with 55 nm of MAE. The averaged pore size was about 50 nm.

To fabricate superhydrophobic SiC surfaces, it is essential to control the surface roughness and morphology. Therefore we combined two etching methods to increase the surface roughness significantly. Since the feature surface (e.g. along the wall) by MAE etching may have more dangling bonds, so the exposed surfaces that are generated by the MAE etching but located beneath the top surface may exhibit higher chemical reactivity. Therefore the etching depth of combined etchings was greatly enhanced compared with RIE or MAE only. The R_q and R_{max} are 72.3 and 471 nm, respectively. Moreover, the pore size increased to ∼100 nm, which allows more air to be trapped within the unit structures.

3.2. Surface treatment

The silane treatment was performed to further lower the surface energy of porous SiC (figure 3). The surface treatment of PFOS is critical to achieve superhydrophobic surfaces. XPS was used to study the surface chemical composition before and after silane treatment. Figure S1 (available at stacks.iop.org/Nano/23/255703/mmedia) shows the XPS survey of porous SiC with combined etchings before and after hydrophobic treatment. The Si, C, O, and F peaks have been identified in both untreated and treated SiC spectra. The O_{1s} peaks of ∼533.3 eV indicates that the surface oxygen exists in the form of hydroxyls, which are capable of reacting with PFOS. The F_{1s} peak in untreated SiC may be due to the etchant residual (HF or H_2SiF_6). After treatment, the F_{1s} peak becomes intense as a result of the introduction of the PFOS layer which contains CF_2 and CF_3 groups. The existence of the PFOS layer is also confirmed by high resolution C_{1s} spectra as show in figure 4. Before treatment, only peaks from SiC (283.4 eV) and CH_2 (285.6 eV) groups are observed. After treatment, new peaks of 293.9 and 291.6 eV appear which can be attributed to CF_3 and CF_2 groups. Moreover, the peak of SiC is suppressed after treatment, possibly due to the dense PFOS coating.

We compared the contact angles on SiC fabricated by different etching methods. After hydrophobic treatment, the contact angle of MAE-SiC was 110.8°. For RIE-SiC, the contact angle was 168° with a large hysteresis of ∼28.4°, as shown in table 3. The high contact angle and low contact angle hysteresis indicate a combined Wenzel–Cassie state (drops that are partially in the Cassie and partially in the Wenzel state), which is probably due to the low etching depth. Thus there is not enough air trapped in the gap between etched

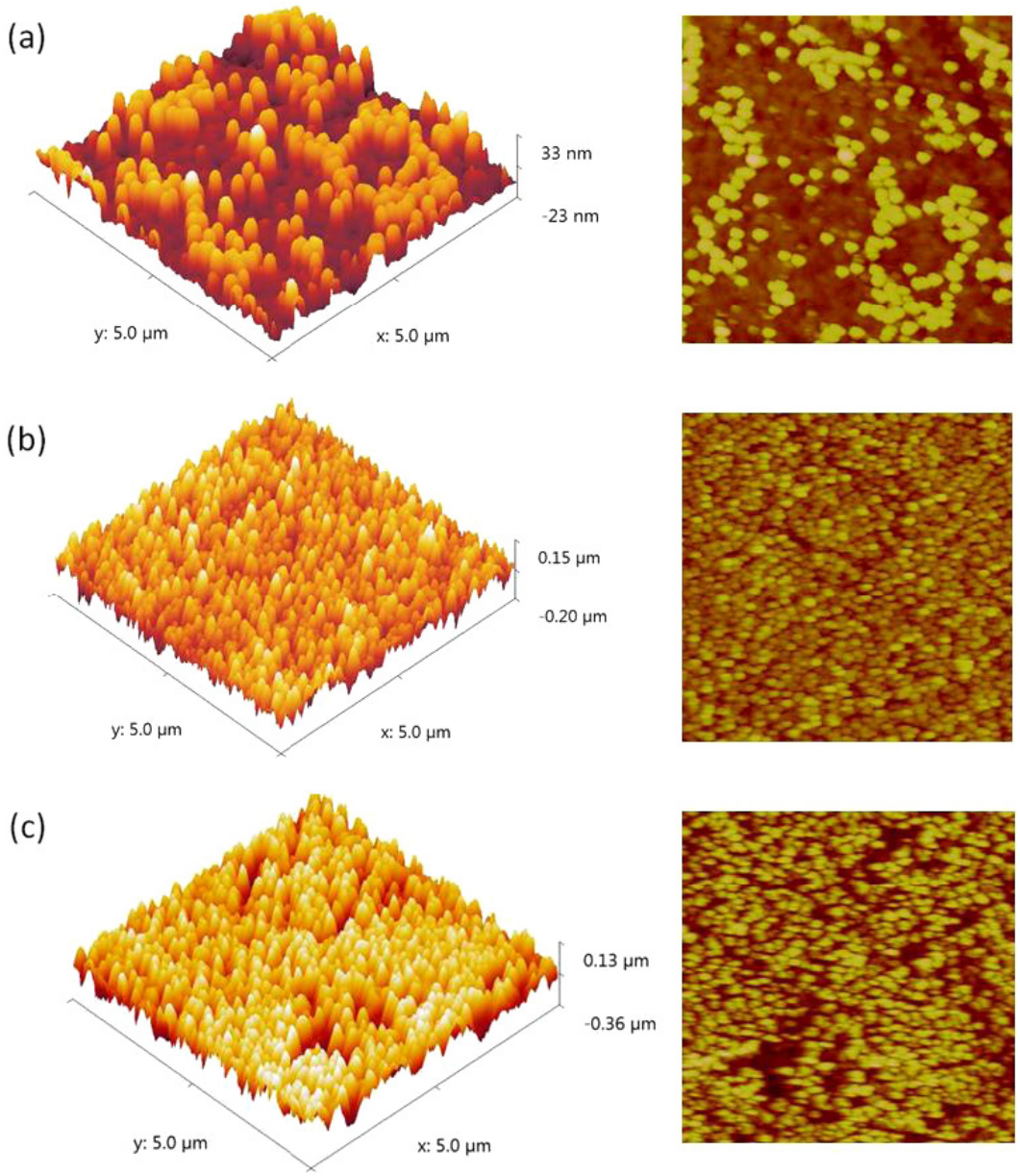

Figure 2. Three-dimensional and one-dimensional AFM images of SiC using different etching methods (a) MAE, (b) RIE and (c) combined MAE and RIE.

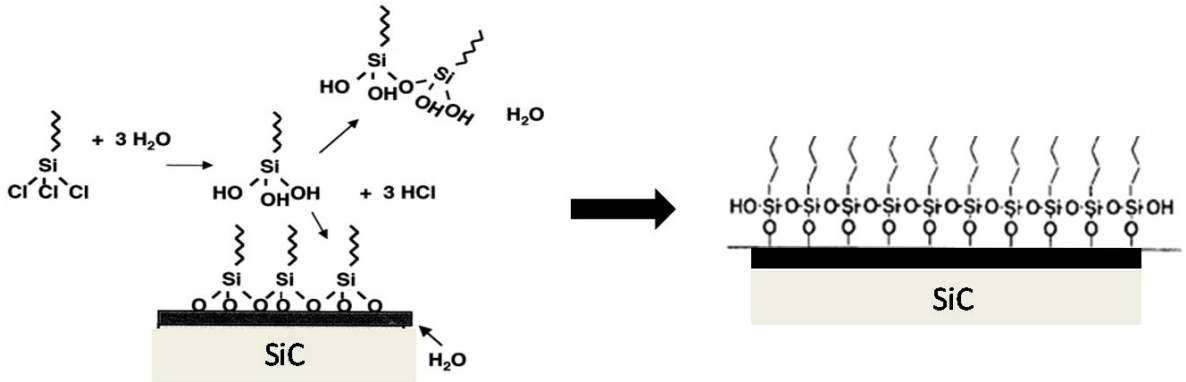

Figure 3. Illustration of PFOS treatment on SiC.

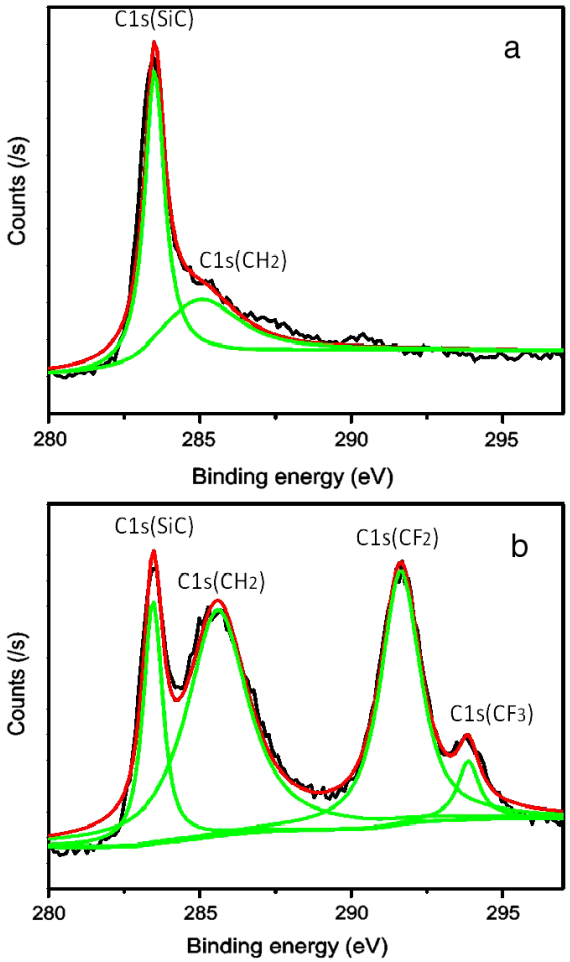

Figure 4. High resolution C 1s spectra of (a) porous SiC before silane treatment, (b) porous SiC after silane treatment.

Table 3. Contact angle and hysteresis of hydrophobic treated rough SiC surfaces.

	MAE	RIE	MAE + RIE
Contact angle (deg)	117.9 ± 1.1	168.1 ± 0.8	169.7 ± 0.9
Contact angle hysteresis (deg)	—	28.4 ± 0.7	2.4 ± 0.2

structures to achieve low hysteresis superhydrophobicity. After combined etchings and silane treatment, the contact angle was 169.7° and hysteresis reduced to only 2.4°. This low hysteresis indicates a Cassie state, and a self-cleaning porous SiC surface. The increased surface roughness and pore size greatly enhanced the air trapping volume within each unit structure, which contributes to the high contact angle and low contact angle hysteresis.

The effect of combined etchings could also be explained in terms of Laplace pressure. The Laplace pressure maintains a composite interface by confining the water at the air/water interface, which can be described as [9]

$$\Delta p = p - p_0 = -\frac{\gamma \cos(\theta - \alpha)}{R_0 + h \tan \alpha}$$

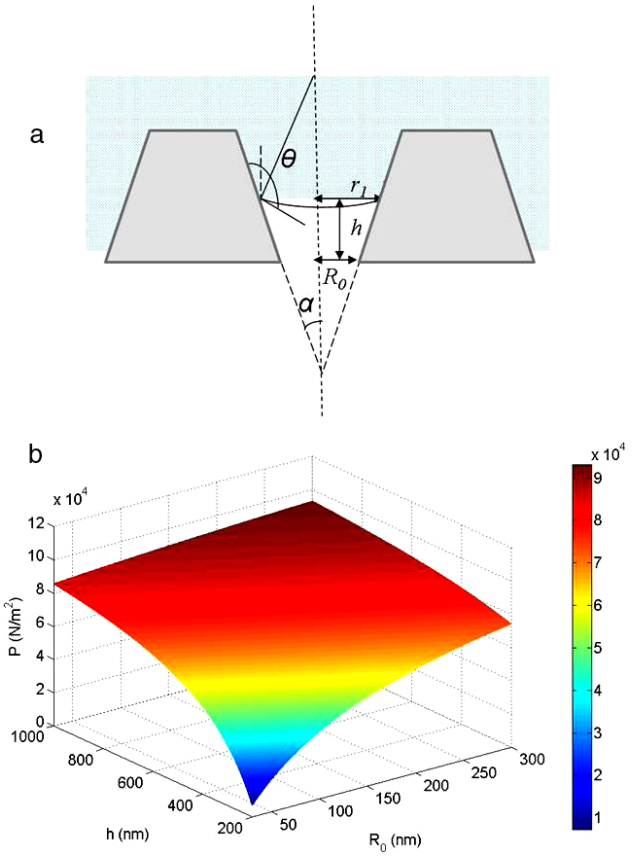

Figure 5. (a) Water contact at surface structures with inclined walls. (b) Laplace pressure (p) changes with height (h) and half width of two adjacent inclined walls (R_0).

where γ is the surface tension of water, θ is Young's contact angle of liquid on the surface, α is the inclination angle, h is the height as illustrated in figure 5(a), R_0 is half of the width between base edges of two adjacent inclined walls, p is the pressure on the liquid side of the meniscus, and p_0 is atmospheric pressure.

Superhydrophobicity is achieved through the formation of a composite interface (solid/water and air/water interfaces) with air trapped within the structure. The Laplace pressure can affect the hysteresis and the transition between a Cassie state and a Wenzel state. For two inclined walls with a certain inclination angle α and Young's contact angle, the increase of R_0 or h increases the Laplace pressure and allows more air trapping between unit structure, and therefore prevents the meniscus approaching the structure bottom. As a result, surface hydrophobicity was enhanced, and an increased apparent contact angle and reduced contact angle hysteresis (reduced contact area) will be achieved. The Laplace pressure of RIE and combined etching are estimated to be 1.07×10^4 Pa and 3.83×10^4 Pa respectively. Compared with RIE only, the combined etching increases both R_0 and h, therefore Laplace pressure is increased (figure 5(b)) and contact angle hysteresis was reduced significantly. But we need to notice that the parameter R_0 cannot be increased too much without increasing h, otherwise the central part of the droplet will touch the bottom of the structure, and the Cassie state will be lost.

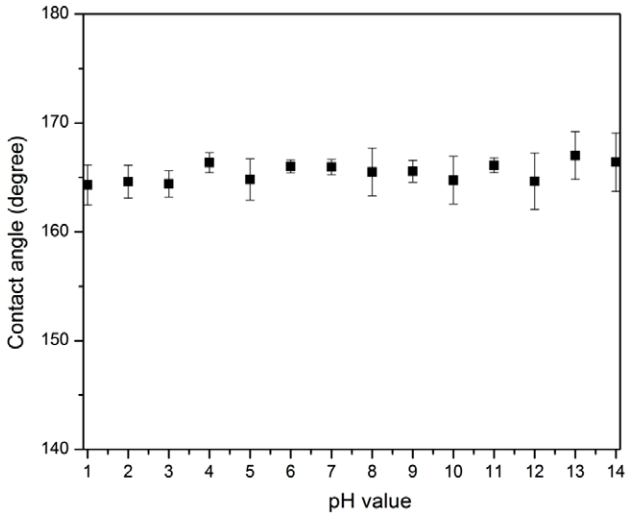

Figure 6. The relationship between pH and the CA on a porous SiC surface by MAE and RIE combined etching.

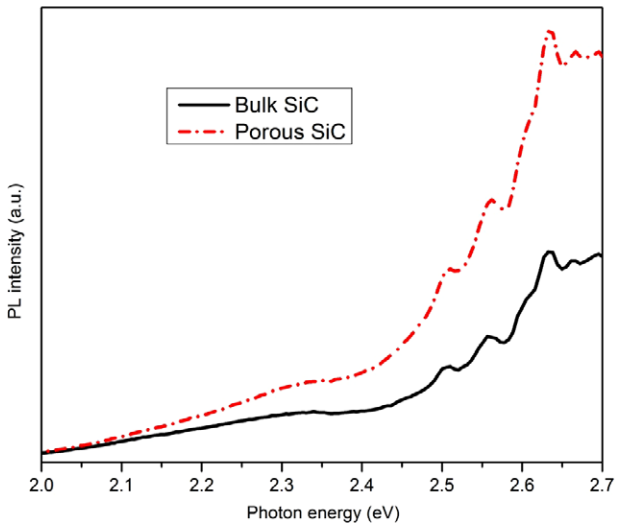

Figure 7. PL intensity of bulk SiC and etched porous SiC (etched by combined MAE and RIE).

3.3. The robustness of superhydrophobic SiC

In order to test the robustness of superhydrophobic surfaces, the superhydrophobic SiC was put in an 85/85 (85 °C, 85% humidity) chamber. It was found that after four weeks the surface maintained the superhydrophobic property and showed a water contact angle (CA) of 165.2°.

The SiC surface also showed superhydrophobicity to corrosive acid/base solutions with pH ranging from 1 to 14. Figure 6 shows the relationship between pH and CA on the superhydrophobic SiC surfaces. CAs remained larger than 160° when the pH of the droplet varied from 1 to 14, and no obvious fluctuation was observed. This indicates that pH values of the aqueous solution have little or no effect on CAs for superhydrophobic SiC surfaces.

3.4. Luminescence property

Bulk SiC has a low emission intensity due to its indirect band gap. It is expected that nanoporous SiC exhibits a similar emission peak or shifted new emission peaks, because of the decreased particle size to the nanometer regime [29]. The luminescent spectra of porous SiC usually span a wide spectrum range from near UV to 600 nm. Many studies reported an increase in photoluminescence intensity was found in the 460–500 nm region of the spectrum upon etching [30]. In our study, the peaks for both bulk SiC and the porous SiC after combined etchings are at 471 nm, and no obvious peak blue shift was observed. This may be due to the large size of the porous structures generated by combined etchings, and therefore no quantum confinement effect was generated [31]. The luminescence intensity is increased three times compared with the bulk one (figure 7). The increasing PL intensity reflects the nanocrystalline size of the pores, and is related to the number of nanocrystals. Since SiC has good biocompatibility, the high surface area and efficient luminescence of porous SiC may have potential applications in biolabeling and biosensing areas.

4. Conclusions

In summary, a large-scale superhydrophobic porous SiC was fabricated by combining Pt-assisted chemical etching and RIE. The surface roughness and air trapping volume of SiC increased significantly after combined etching. As a result, a high contact angle of 169.7° and low hysteresis of 2.4° self-cleaning SiC surface was generated, which is very stable in different pH solutions. The luminescent intensity of porous SiC was enhanced compared with bulk materials. Such stable superhydrophobic porous SiC surfaces may have potential applications for microfluid channels, thermal ground planes, sensors, etc even under hostile environments.

Acknowledgments

The authors acknowledge financial support from the National Science Foundation (NSF CMMI No. 0422553) and the National Electric Energy Testing Research and Applications Center (NEETRAC) at the Georgia Institute of Technology.

References

[1] Zhuang D and Edgar J H 2005 *Mater. Sci. Eng.* R **48** 1
[2] Wu K H, Fang Y K, Hsieh W T, Ho J J, Lin W J and Hwang J D 1998 *Electron Lett.* **34** 2243
[3] Connolly E J, Timmer B, Pham H T M, Groeneweg J, Sarro P M, Olthuis W and French P J 2005 *Sensors Actuators* B **109** 44
[4] Shwop J E 1962 *Advisory Group on Electron Tubes* vol 1 (New York: Engineering Publishers)
[5] Rosso M, Arafat A, Schroen K, Giesbers M, Roper C S, Maboudian R and Zuilhof H 2008 *Langmuir* **24** 4007
[6] Xiu Y H, Zhang S, Yelundur V, Rohatgi A, Hess D W and Wong C P 2008 *Langmuir* **24** 10421
[7] Lafuma A and Quere D 2003 *Nature Mater.* **2** 457
[8] Lin Z Y, Liu Y and Wong C P 2010 *Langmuir* **26** 16110
[9] Xiu Y H, Zhu L B, Hess D W and Wong C P 2007 *Nano Lett.* **7** 3388

[10] Liu Y, Xiu Y H, Hess D W and Wong C P 2010 *Langmuir* **26** 8908
[11] Liu Y, Xiu Y H, Hess D W and Wong C P 2010 *Proc. IEEE 60th Electronic Components Technology Conf.* p 1719
[12] Liu Y, Das A, Xu S, Lin Z Y, Xu C, Wang Z L, Rohatgi A and Wong C P 2012 *Adv. Energy Mater.* **2** 247
[13] Niu J J and Wang J N 2009 *J. Phys. Chem.* B **113** 2909
[14] Niu J J, Wang J N and Xu Q F 2008 *Langmuir* **24** 6918
[15] Wang J J, Lambers E S, Pearton S J, Ostling M, Zetterling C M, Grow J M, Ren F and Shul R J 1998 *Solid State Electron* **42** 2283
[16] Boukezzata A *et al* 2010 *Appl. Surf. Sci.* **256** 5592
[17] Kato M, Ichimura M, Arai E and Ramasamy P 2003 *Jpn. J. Appl. Phys.* **42** 4233
[18] Bourenane K, Keffous A, Nezzal G, Boukezzata A and Naama S 2007 *Surf. Interface Anal.* **39** 392
[19] Chang W H, Schellin B, Obermeier E and Huang Y C 2006 *J. Microelectromech. Syst.* **15** 548
[20] Rittenhouse T L, Bohn P W and Adesida I 2003 *Solid State Commun.* **126** 245
[21] Chuah L S, Hassan Z and Abu Hassan H 2007 *Optoelectron. Adv. Mater.* **1** 400
[22] Diaz D J, Williamson T L, Guo X Y, Sood A and Bohn P W 2006 *Thin Solid Films* **514** 120
[23] Cao L H, Li B H and Zhao J H 1998 *J. Electrochem. Soc.* **145** 3609
[24] Yih P H, Saxena V and Steckl A 1997 *J. Phys. Status Solidi* b **202** 605
[25] Bardwell J A, Webb J B, Tang H, Fraser J and Moisa S 2001 *J. Appl. Phys.* **89** 4142
[26] Cho H, Auh K H, Han J, Shul R J, Donovan S M, Abernathy C R, Lambers E S, Ren F and Pearton S J 1999 *J. Electron Mater.* **28** 290
[27] Scofield J D, Bletzinger P and Ganguly B N 1998 *Appl. Phys. Lett.* **73** 76
[28] Camara N and Zekentes K 2002 *Solid State Electron* **46** 1959
[29] Fan J Y, Wu X L and Chu P K 2006 *Prog. Mater. Sci.* **51** 983
[30] Botsoa J, Bluet J M, Lysenko V, Marty O, Barbier D and Guillot G 2007 *J. Appl. Phys.* **102** 083526
[31] Petrovakoch V, Sreseli O, Polisski G, Kovalev D, Muschik T and Koch F 1995 *Thin Solid Films* **255** 107